Chinese Chemical Letters 36 (2025) 110760

Contents lists available at ScienceDirect

Chinese Chemical Letters

journal homepage: www.elsevier.com/locate/cclet

Modified triphenylamine donors with shallower HOMO energy levels to construct long-wavelength TADF emitters of efficient organic light-emitting diodes

Hao Zhuo[a], Ming Zhang[a], Hengyuan Zhang[a], Hui Lin[a], Gang Yang[a], Silu Tao[a], Caijun Zheng[a,*], Xiaohong Zhang[b]

[a] School of Optoelectronic Science and Engineering, University of Electronic Science and Technology of China, Chengdu 610054, China
[b] Institute of Functional Nano & Soft Materials (FUNSOM), Soochow University, Suzhou 215123, China

ARTICLE INFO

Article history:
Received 25 September 2024
Revised 9 December 2024
Accepted 12 December 2024
Available online 13 December 2024

Keywords:
Organic light-emitting diodes
Thermally activated delayed fluorescence
Long-wavelength emission
Triphenylamine
Shallow HOMO energy level

ABSTRACT

Triphenylamine (TPA) is the most promising donor fragment for the construction of long-wavelength thermally activated delayed fluorescence (TADF) emitters owing to its suitable dihedral angle that could enhance radiative decay to compete with the serious non-radiative decay. However, the moderate electron-donating capacity of TPA seriously limits the selection of acceptor for constructing long-wavelength TADF emitters with narrow bandgaps. To address this issue, in this work, the peripheral benzene of TPA was replaced with 1,4-benzodioxane and anisole to obtain two new electron-donating units *N*-(2,3-dihydrobenzo[*b*][1,4]dioxin-6-yl)-*N*-phenyl-2,3-dihydrobenzo[*b*][1,4]dioxin-6-amine (TPADBO, −5.02 eV) and 4–methoxy-*N*-(4-methoxyphenyl)-*N*-phenylaniline (TPAMO, −5.00 eV), which possess much shallower highest occupied molecule orbital (HOMO) energy levels than the prototype TPA (−5.33 eV). Based on TPA and the modified TPA donor fragments, three TADF emitters were designed and synthesized, namely Py-TPA, Py-TPADBO and Py-TPAMO, with the same acceptor fragment 12-(2,6-diisopropylphenyl)pyrido[2′,3′:5,6]pyrazino[2,3-*f*][1,10]phenanthroline (Py). Among them, Py-TPAMO exhibits the highest photoluminescence quantum yield of 78.4% and the smallest singlet-triplet energy gap, which is because the introduction of anisole does not cause significant molecule deformation for the excited Py-TPAMO. And Py-TPAMO-based OLEDs successfully realize a maximum external quantum efficiency of 25.5% with the emission peak at 605 nm. This work provides a series of candidate of donor fragments for the development of efficient long-wavelength TADF emitters.

Long-wavelength organic light-emitting diodes (OLEDs) with red, deep-red and near-infrared (DR/NIR) emission play important roles not only in the common fields of flat panel displays and lighting devices, but also in night vision devices, optical communication and information security [1–4]. Consequently, long-wavelength emitters have drawn great attention in recent years. Among the general OLED emitters, conventional fluorescent compounds and phosphorescent metal complexes usually suffer the dilemma of low exciton utilization and high cost of precious metals [5–8]. It was not until 2012 that the thermally-activated delayed fluorescence (TADF) emitters emerged as the most promising candidates for the development of long-wavelength emitters, due to their theoretical exciton utilization up to 100% and pure organic chemical structures [9–18]. However, according to the energy gap law, the non-radiative decay exponentially increases with the decrease of the bandgap [19–21]. Therefore, long-wavelength TADF emitters have to address serious non-radiative decays due to their extremely small energy bandgaps. Till now, how to develop efficient long-wavelength TADF emitters is still of urgency and importance.

In general, the narrow energy bandgaps of long-wavelength TADF emitters can be realized by modulating the donor or acceptor strength of the molecule to enhance the charge transfer (CT) properties [22,23]. Currently, many acceptor fragments with deep lowest unoccupied molecular orbital (LUMO) energy levels have been developed by extending π-conjugated system and introducing electron-deficient substituents (such as cyan units, sulfonyl and fluorine atoms) [24–27]. However, the donor fragments that can be matched are limited [28]. Especially for long-wavelength TADF emitters, triphenylamine (TPA) is the most commonly used donor prototype fragment. Compared with other donor fragments,

* Corresponding author.
E-mail address: zhengcaijun@uestc.edu.cn (C. Zheng).

https://doi.org/10.1016/j.cclet.2024.110760
1001-8417/

TPA can form a moderate donor-acceptor dihedral angle (30°–60°), making it is easier to induce strong conjugation with the acceptor unit, which ensures that the radiative transition process occurs efficiently [29–32]. Unfortunately, prototype TPA only has moderate electron-donating capacity and needs to be elaborately matched with strong acceptor fragments to achieve strong CT transition, which has greatly hindered the development of long-wavelength TADF emitters. In general, tuning of the highest occupied molecular orbital (HOMO) energy level can be achieved by expanding the π-conjugated system and introducing electron-rich substituents. Inspired by this, great efforts have been made to modify TPA fragment to enhance its electron-donating capacity without inducing any potential drawbacks (Fig. S1 in Supporting information) [33–40]. For example, Yin *et al.* modified TPA fragment by introducing benzofuran to replace the peripheral benzene ring of TPA as a donor fragment [40]. Zhang and his colleagues utilized a bulky fluorene to anchor the rotatable biphenyl portion in the TPA unit [39]. However, the above modulations can only slightly improve the electron-donating ability of TPA-based donors (the up-regulations of HOMO energy levels are below 0.2 eV), which is insufficient to fulfill the ambition of obtaining efficient lower-energy band emitter materials. Therefore, to realize stronger a CT transition, it is necessary to explore stronger electron donor fragments to meet the requirements for the design of long-wavelength emitters.

In this work, TPA-based strong donor fragments were designed and theoretical evaluated based on density functional theory (DFT). Specifically, electron-rich groups including benzo[*b*]thiophene, 1,4-benzodioxane and anisole were introduced, and naphthalene, pyrene and quinoline were incorporated into the TPA fragment to expand the conjugation system (Fig. S2 in Supporting information) [41,42]. Considering the degree of enhancement of the electron-donating ability, 1,4-benzodioxane and anisole were finally employed to modify prototype TPA fragments and synthesized to obtain *N*-(2,3-dihydrobenzo[*b*][1,4]dioxin-6-yl)-*N*-phenyl-2,3-dihydrobenzo[*b*][1,4]dioxin-6-amine (TPADBO) and 4–methoxy-*N*-(4-methoxyphenyl)-*N*-phenylaniline (TPAMO) fragments. Subsequently, 12-(2,6-diisopropylphenyl)pyrido[2′,3′:5,6]pyrazino[2,3-*f*][1,10]phenanthroline (Py) was used as the acceptor to obtain the two new TADF emitters Py-TPADBO and Py-TPAMO, respectively. For comparison, the prototype molecule (4,4′-(12-(2,6-diisopropylphenyl)pyrido[2′,3′:5,6]pyrazino[2,3-*f*][1,10]phenanthroline-3,6-diyl)bis(*N*,*N*-diphenylaniline (Py-TPA) with the same acceptor fragment but unmodified TPA fragment was also synthesized. As expected, due to the modification with electron-rich oxygen atoms, Py-TPADBO (−5.02 eV) and Py-TPAMO (−5.00 eV) exhibit much shallower HOMO than Py-TPA (−5.33 eV), and thus Py-TPADBO and Py-TPAMO exhibit more red-shifted emissions. In addition, the modification of the electron-rich groups increases the dihedral angle of the donor and acceptor fragments, which further resulted in a small singlet-triplet energy gap (ΔE_{ST}). More significantly, the introduction of anisole resulted in the least deformation of Py-TPAMO, with a high photoluminescence quantum yield (PLQY) of 78.4%. Thanks to its superior photoluminescence property, Py-TPAMO enables its OLED to reach a maximum external quantum efficiency (EQE) of 25.5% with a peak red emission of 605 nm. Surprisingly, Py-TPAMO-based OLED has a red-shifted electroluminescence spectrum but higher device efficiency than both Py-TPA- and Py-TPADBO-based OLEDs. In conclusion, this work broadens the range of electron-donating energy levels of TPA-based donor fragments and provides diverse options for the design of high-efficiency long-wavelength TADF-OLED emitters.

The structures of the target molecules Py-TPAMO and Py-TPADBO, as well as the control molecule Py-TPA, are shown in Scheme 1. All of them employ the same framework Py as the electron acceptor unit. To improve the electron-donating ability of donor fragments, the 1,4-benzodioxane and anisole units were employed to replace the peripheral benzene ring of the TPA moiety respectively. The specific synthesis procedures were described in the supplementary information, and the three compounds were successfully confirmed by nuclear magnetic resonance spectroscopy (Figs. S17-S22 in Supporting information) and high-resolution mass spectrometry characterization. Thermogravimetric analysis and differential scanning calorimetry confirmed the thermal stability of the three compounds. As shown in Fig. S3 (Supporting information), these three compounds have a similar decomposition temperature of roughly 420 °C, and the glass tran-

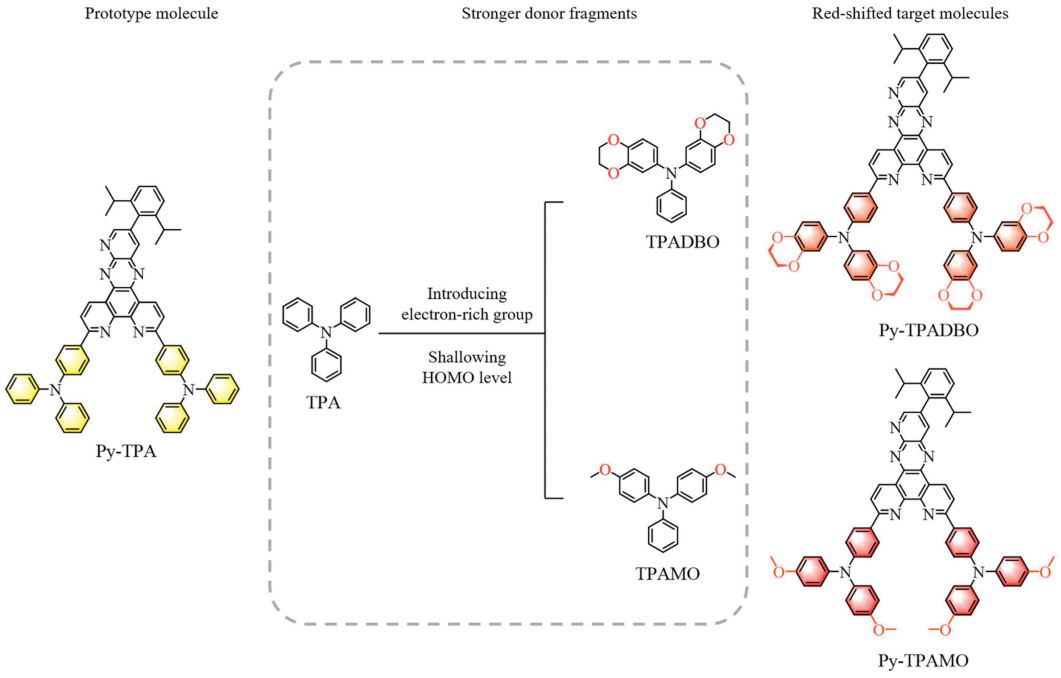

Scheme 1. The design concept for Py-TPA, Py-TPADBO and Py-TPAMO.

sition temperatures were 202 °C, 198 °C and 223 °C for Py-TPA, Py-TPADBO and Py-TPAMO, respectively, which ensure their stability during the thermal evaporation process.

The electronic distributions of molecule orbitals and optimized ground and excited state structures of Py-TPA, Py-TPADBO and Py-TPAMO were evaluated by the DFT and time-dependent DFT (TD-DFT) based on the B3LYP/6–31G(d) set, as shown in Fig. S4 and Table S1 (Supporting information). The similarities between the frontier molecule orbital of the three molecules are mainly exhibited in their LUMO distributions, which are localized on the Py fragment. Moreover, the introduction of 1,4-benzodioxane and anisole lead to the HOMO distribution of Py-TPADBO and Py-TPAMO extended to the periphery of the donor moiety cores, aligning with their HOMO energy levels are −4.95 eV, −4.65 eV, and −4.67 eV, respectively. In addition, LUMO, LUMO+1 of three molecules have similar distribution pattern on the acceptor core and HOMO, HOMO-1 on the surrounding TPA derivatives also have similar pattern, which means the three molecules have two pair of *quasi*-degenerate occupied and unoccupied molecular orbitals according to the DFT calculation, as shown in Figs. S5-S7 (Supporting information). The similar distribution pattern endows CT characteristics of occupied and unoccupied orbitals and contributes to the fast reverse intersystem crossing (RISC) process between the high-order triplet excited states and the singlet excited states, as shown in Fig. S4.

In addition, the dihedral angles (θ) between the planar acceptor moiety and the propeller-shaped donor moiety in the ground state geometry were 14.0°, 12.4° and 15.4°, corresponding to Py-TPA, Py-TPADBO and Py-TPAMO, respectively. As shown in Fig. S4, for the excited singlet state (S_1) and excited triplet (T_1) state configuration, the dihedral angle between D-A rose to 17.2°/17.5°, 26.1°/26.3°, and 33.2°/25.1°, respectively. Compared with the prototype molecule Py-TPA, the dihedral angles of the donor and acceptor segments of Py-TPADBO and Py-TPAMO were significantly increased because the introduced oxygen atoms generate a greater repulsive force between neighboring molecules thus causing a larger torsion angle. As a result, the torsion angle increased by introducing the 1,4-benzodioxane and anisole units in the triarylamine moiety, which could conducive to reduce the spatial overlap between HOMO and LUMO, thereby achieving a relatively smaller ΔE_{ST} potentially. Correspondingly, the theoretical values of ΔE_{ST} are also consistent with the trend of dihedral angle, that is, the single-triplet energy gaps of Py-TPADBO (0.17 eV) and Py-TPAMO (0.16 eV) are smaller than that of Py-TPA (0.20 eV), as shown in Table S1. Thus, the introduction of oxygen-containing groups increased the HOMO level by approximately 0.3–0.4 eV, which further enhanced the intermolecular CT interactions. Consequently, the corresponding ΔE_{ST} decreased, which benefits the fast RISC process. Further, the natural transition orbitals of Py-TPA, Py-TPADBO and Py-TPAMO are visualized in Fig. S8 (Supporting information), it is clearly observed that all the excited states exhibit CT-dominated features.

In addition, it is essential to evaluate the degree of molecular deformation during the transition from ground to excited states to suppress non-radiative energy loss caused by conformational relaxation or molecular motion [43]. The optimized S_1/T_1 conformation of Py-TPA, Py-TPADBO and Py-TPAMO revealed that the three molecules undergo different degrees of distortion after excitation, especially the greater the volume of oxygen-containing groups attached to the peripheral benzene ring, the more obvious the degree of molecular deformation was observed. As shown in Fig. S4, each molecule had two TPA-based donor fragments, where the torsion angles between neighboring benzene rings in each triarylamine were labeled α, β and γ, respectively. For the excited Py-TPA configuration, the torsion angle (α) between the two free-rotating benzene rings in the TPA group far from the receptor group changed from a minimum value of 35.7° to a maximum value of 51.1°. For the excited Py-TPADBO configuration, β increased from a minimum value of 32.2° to a maximum value of 65.7°. For the excited Py-TPAMO configuration, the minimum ground state and excited state torsion angles (γ) changed from a minimum value of 28.6° to a maximum value of 56.2°. For both S_1 and T_1 states, Py-TPADBO showed the most severe excited state deformation compared to the other two molecules, which may be attributed to the greater repulsion of neighboring identical 1,4-benzodioxane units. Moreover, the closed alkyl group of 1,4-benzodioxane unit could induce distortion of the peripheral benzene ring, resulting in further distortion of the donor part, greatly increasing the possibility of vibrational relaxation and ultimately causes serious non-radiative energy loss. The slight degree of excited state deformation observed in Py-TPAMO is conducive to reducing the occurrence of vibrational relaxation further suppressing the non-radiative decay process.

Subsequently, the root-mean-square displacements (RMSDs) between ground state (S_0), S_1 and T_1 were also calculated to theoretically evaluate the geometric changes (Fig. S9 in Supporting information). The RMSDs between S_0 and S_1, S_0 and T_1, and S_1 and T_1 for the prototype molecule Py-TPA were 0.314 Å, 0.200 Å, and 0.210 Å, respectively. The worst geometric variations of the Py-TPADBO were 0.783 Å for S_0-S_1, 0.695 Å for S_0-T_1 and 0.124 Å for S_1-T_1. While Py-TPAMO possessed the same excellent geometric variation as Py-TPA between S_0, S_1 and T_1 were obtained, which were 0.389 Å for S_0-S_1, 0.319 Å for S_0-T_1 and 0.088 Å for S_1-T_1. Obviously, the RMSD results are almost similar to the degree of deformation of the three excited molecules. Since the slight geometrical variation of Py-TPAMO between the ground state and the excited state contributes to the suppression of structural relaxation, it is expected that Py-TPAMO will undergo a relatively slow non-radiative decay process [44].

Further, to confirm the enhancement of donor strength, the electrochemical properties of Py-TPA, Py-TPADBO and Py-TPAMO molecules were further characterized by cyclic voltammetry. As shown in Fig. 1a and Table S2 (Supporting information), all three molecules showed very similar reduction curves with estimated LUMO levels of −3.24 eV, −3.17 eV and −3.19 eV, respectively, determined from the reduction onsets. These results are well in line

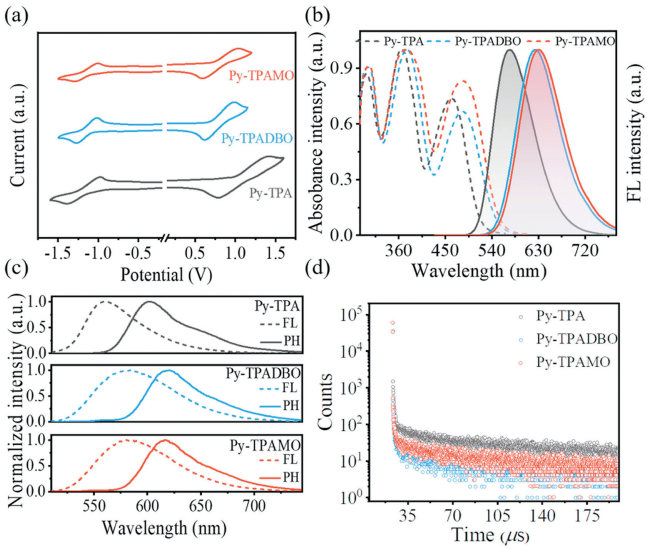

Fig. 1. (a) Cyclic voltammetry diagram of Py-TPA, Py-TPADBO and Py-TPAMO in dichloromethane (DCM). (b) Normalized absorption and fluorescence spectra of Py-TPA, Py-TPADBO and Py-TPAMO in toluene at room temperature (10^{-5} mol/L). (c) Normalized fluorescence and phosphorescence spectra in dilute toluene solution (10^{-5} mol/L) at 77 K. (d) Transient PL decay curves of doped films (1 wt% in CBP) at room temperature.

with their identical acceptor segments. While the HOMO energy levels of Py-TPADBO (−5.02 eV) and Py-TPAMO (−5.00 eV) were estimated to be much shallower than that of Py-TPA (−5.33 eV), indicating that the electron-donating ability of the TPADBO and TPAMO segments was evidently enhanced compared to that of TPA. The corresponding to optical band gaps of Py-TPA, Py-TPADBO, and Py-TPAMO were 2.09 eV, 1.85 eV, and 1.81 eV, respectively, implying that Py-TPADBO and Py-TPAMO will have more red-shifted emission bands relative to Py-TPA. These results show that the modified TPADBO and TPAMO donor fragments have a greater potential to construct long-wavelength emitters.

The photophysical properties of Py-TPA, Py-TPADBO and Py-TPAMO molecules were investigated to demonstrate the spectroscopic effects resulting from the enhanced electron-donating ability of the TPA-based derivatives. The ultraviolet-visible absorption characterization of the three molecules in dilute toluene solution was further investigated. As shown in Fig. 1b, the absorption spectra of all the three molecules consisted of two main absorption bands. The intense high-energy absorption bands with peaks around 360 nm could be ascribed to the π-π^* transitions from their local excited states, and the broad low-energy absorption bands from 410 nm to 560 nm were attributed to the intramolecular charge transfer (ICT) transition from TPA-based derivatives to Py acceptor. Owing to the different electron-donating abilities of the TPA-based derivatives (TPAMO > TPADBO > TPA), the ICT absorption spectra of Py-TPAMO and Py-TPADBO were located in a red-shifted wavelength range of 428–592 nm and 427–526 nm, respectively, compared to Py-TPA (411–538 nm). Moreover, all three molecules displayed a board and structureless photoluminescence (PL) spectra with emission peaks at 571 nm, 623 nm and 630 nm, respectively. Besides, the photoluminescence spectra of Py-TPA, Py-TPADBO and Py-TPAMO in different solvents are demonstrated in Fig. S10 (Supporting information). A significant red-shifted emission due to ICT transition was observed with increasing solvent polarity, indicating that the three molecules have typical TADF characteristics [45].

To further investigate the energy levels of the S_1 and T_1 states, the fluorescence and phosphorescence of the three emitters were further measured at 77 K (Fig. 1c). The energy levels of S_1/T_1 states are estimated to be 2.22/2.06 eV for Py-TPA, 2.14/2.00 eV for Py-TPADBO and 2.13/2.01 eV for Py-TPAMO, as deduced from their emission spectral peaks. Correspondingly, the ΔE_{ST} can be calculated to be 0.16 eV, 0.14 eV, and 0.12 eV for Py-TPA, Py-TPADBO, and Py-TPAMO, respectively (Table S2). Apparently, the small singlet-triplet energy band gap proves that all three emitters possess TADF properties. It is clear that the modification of triarylamine using oxygen-containing substituents not only further enhances the electron-donating ability but also significantly strengthens the distribution of HOMO and LUMO, resulting in a smaller ΔE_{ST}. The Py-TPAMO could be expected to exhibit a relatively fast RISC process. Furthermore, the PLQYs of Py-TPA, Py-TPADBO and Py-TPAMO were measured in doped films under a nitrogen atmosphere and estimated to be 77.3%, 50.5%, and 78.4%, respectively, by using an integrating sphere. And the PLQY value of Py-TPADBO was the worst among all three emitters, probably due to the apparent vibrational relaxation.

Further, the transient PL decay properties of Py-TPA, Py-TPADBO and Py-TPAMO m were then measured at room temperature. As expected, these molecules exhibit both nanosecond-scale prompt fluorescence and microsecond-scale delayed fluorescence decay components at room temperature, which endow their obvious TADF property. Specifically, the prompt/delayed lifetimes were evaluated to be 8.08 ns/82.45 µs for Py-TPA, 11.57 ns/93.18 µs for Py-TPADBO and 11.28 ns/64.48 µs for Py-TPAMO at room temperature (Fig. 1d and Fig. S11 in Supporting information). Apparently, the shortest τ_d exhibited for Py-TPAMO-doped films should be attributed to the smaller ΔE_{ST}, indicating that Py-TPAMO undergoes a more efficient RISC process. To better understanding these three molecules of photoexcitation processes, the relevant kinetic parameters were further calculated (Table S3 in Supporting information). The rate constants of the RISC process (k_{RISC}) values of Py-TPA, Py-TPADBO and Py-TPAMO are respectively estimated to be $1.10 \times 10^5\ s^{-1}$, $1.15 \times 10^5\ s^{-1}$, and $1.33 \times 10^5\ s^{-1}$, corresponding to the properties of their excited states, with the smallest ΔE_{ST} of Py-TPAMO leading to the fast k_{RISC}. And the rate constants of fluorescence decay (k_F) values of Py-TPA, Py-TPADBO and Py-TPAMO are estimated to be $1.05 \times 10^7\ s^{-1}$, $0.40 \times 10^7\ s^{-1}$, and $0.80 \times 10^7\ s^{-1}$, respectively. The k_F of Py-TPA is higher than that of Py-TPADBO and Py-TPAMO, which may be due to the high oscillator strength of the small D-A dihedral angle of Py-TPA. Moreover, the rate constants of non-radiative decay of singlet excitons (k_{nr}^S) values of Py-TPA, Py-TPADBO and Py-TPAMO are estimated to be $3.08 \times 10^6\ s^{-1}$, $3.97 \times 10^6\ s^{-1}$, and $2.21 \times 10^6\ s^{-1}$, respectively. This result suggests that the rate constants of the non-radiative decay process of Py-TPAMO can be significantly suppressed by introducing small fragments of anisole and its molecular rigidity is also better preserved, which together suppresses the structural relaxation and non-radiative decay, and consequently has the smallest k_{nr}^S. Therefore, it is foreseen that Py-TPAMO could utilize a large number of excitons in OLED.

Finally, the electroluminescence (EL) properties of these three materials were further used to evaluate. And the multilayer OLEDs with 4,4′-di(9*H*-carbazol-9-yl)−1,1′-biphenyl (CBP) and Py-TPA derivatives co-doped as the light-emitting layer were also prepared. As illustrated in Fig. 2a, the devices I-III were fabricated with a structure of ITO (110 nm)/TAPC (35 nm)/TCTA (10 nm)/CBP:(1 wt% emitters) (20 nm)/TmPyPB (55 nm)/LiF (1 nm)/Al (100 nm). Here, ITO and Al are served as the anode and the cathode, respectively; 4,4′-(cyclohexane-1,1-diyl)bis(*N*,*N*-di-*p*-tolylaniline) (TAPC), tris(4-(9*H*-carbazol-9-yl)phenyl)amine (TCTA), 3,3′-(5′-(3-(pyridin-3-yl)phenyl)-[1,1′:3′,1″-terphenyl]−3,3″-diyl)dipyridine (TmPyPB) and LiF are respectively employed as the hole-transporting layer, exciton-blocking layer, electron-transporting layer and electron-injecting layer. The energy diagram and chemical structures of the corresponding molecules used in the devices are shown in Fig. 2a and Fig. S12 (Supporting information), and the key electroluminescence data are summarized in Table 1.

As shown in Figs. S13-S15 and Table S4 (Supporting information), Py-TPA, Py-TPADBO, and Py-TPAMO are doped into the CBP host with different doping concentrations of 1%, 3%, 5%, and 7%, respectively. And all three molecules are optimized for device performance at the very low doping ratio of 1 wt% (Figs. 2b-d, corresponding device I-III). And the emission peaks of the Py-TPADBO,

Table 1
Summary of EL characteristics of the optimal devices.

Devices[a]	λ_{EL} (nm)[b]	V_{on} (V)[c]	Maximum values CE/PE/EQE	Values at 100 cd/m^2 CE/PE/EQE
I	565	3.6	68.7/60.8/20.9	24.9/17.7/7.4
II	585	3.7	40.2/33.7/17.4	19.4/11.9/8.4
III	605	3.7	47.7/40.4/25.5	29.2/18.8/15.2
IV	568	3.2	64.1/62.9/20.7	24.3/17.7/7.5
V	600	3.2	33.9/33.1/18.1	18.2/13.5/8.9
VI	616	3.1	32.7/33.1/23.7	25.0/17.0/16.6

V_{on}: turn-on voltage (V). CE: current efficiency (cd/A). PE: power efficiency (lm/W). EQE: the external quantum efficiency (%).

[a] The light-emitting layer structure of device I-III are as follows: CBP:(1 wt% Py-TPA/Py-TPADBO/Py-TPAMO). The light-emitting layer structure of device IV-VI are as follows: DMIC-TRZ:(1 wt% Py-TPA/Py-TPADBO/Py-TPAMO).

[b] Electroluminescence peaks of the EL spectra at a brightness of 100 cd/m^2.

[c] Turn on voltage at a brightness of 1 cd/m^2.

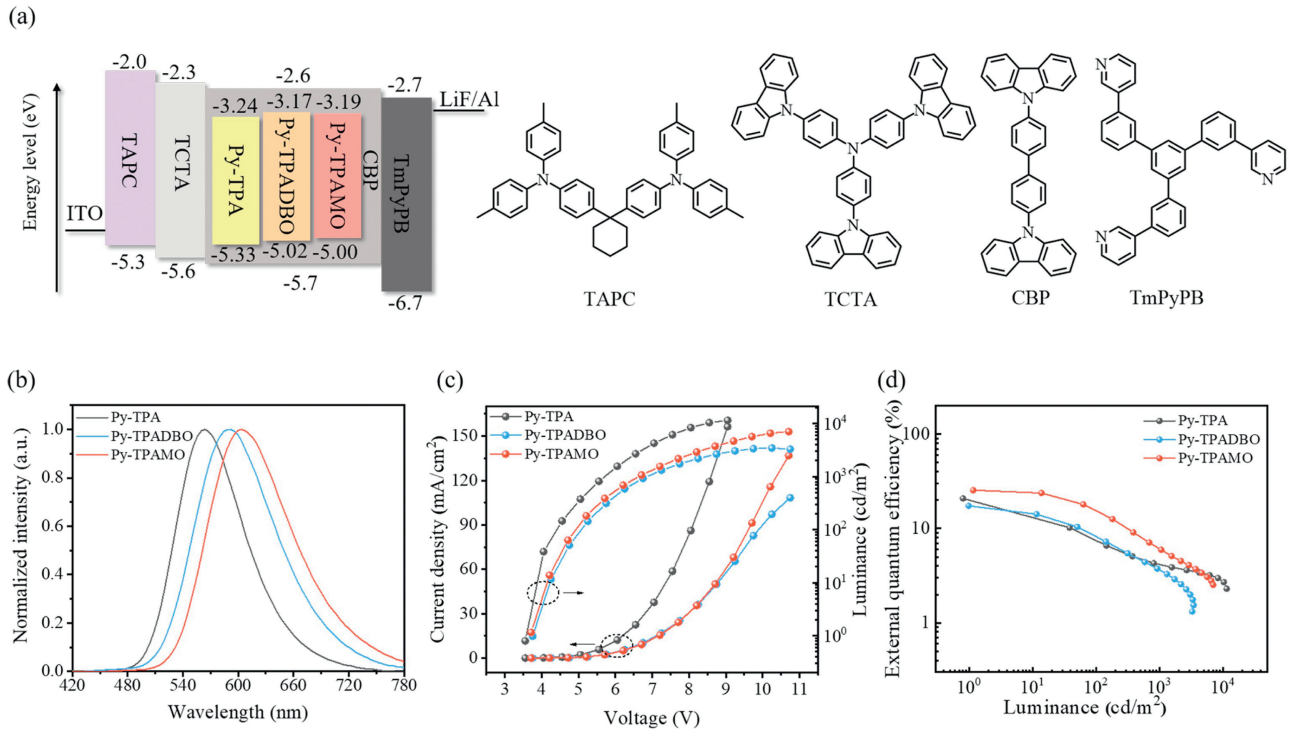

Fig. 2. (a) Energy diagram and chemical structures of the materials used in devices with CBP as the host. (b) EL spectra at 100 cd/m^2, (c) luminance-voltage-current density characteristic curves, and (d) external quantum efficiency–luminance characteristics of Py-TPA, Py-TPADBO and Py-TPAMO-based OLEDs.

and Py-TPAMO devices are significantly red-shifted from that of the Py-TPA by 565 nm, 585 nm, and 605 nm, respectively, due to the further enhanced intermolecular CT interactions. Moreover, the Py-TPADBO and Py-TPAMO emitters exhibit more significant concentration sensitivity in OLEDs than Py-TPA. It may be due to the narrowed bandgap of the emitters, which makes Py-TPADBO- and Py-TPAMO-based devices more susceptible to non-radiative exciton losses [46]. In fact, only Py-TPADBO-based devices indeed exhibit the worst efficiency due to the relatively fast k_{nr}^S. In addition, it was observed that the current density of Py-TPADBO-based and Py-TPA-based OLED is much lower than that of Py-TPA-based OLED, which may be due to the charge trapping phenomenon [47]. Correspondingly, the devices based on Py-TPA, Py-TPADBO, and Py-TPAMO are approaching their optimized maximum EQE values of 20.9%, 17.4% and 25.5%, respectively.

Despite the outstanding maximum EQE values of devices I-III, high turn-on voltages were observed. To reduce the driving voltages, the bipolar host 1,3-dihydro-1,1-dimethyl-3-(3-(4,6-diphenyl-1,3,5-triazin-2-yl)phenyl)indeno[2,1-*b*]carbazole (DMIC-TRZ) was chosen as an alternative to CBP. Accordingly, the bipolar host-based OLED, devices IV-VI were fabricated with a configuration of ITO/TAPC (35 nm)/TCTA (10 nm)/DMIC-TRZ:(1 wt% emitters) (20 nm)/TmPyPB (55 nm)/LiF (1 nm)/Al (100 nm). As shown in Fig. S16 (Supporting information) and Table 1, benefiting from the promoted carrier injection, the V_{on} of devices I-III was reduced by 0.4–0.6 V compared with that of devices IV-VI. In addition, the excellent maximum EQE values were maintained with the significantly reduced driving voltages, that is, the DMIC-TRZ-based devices with Py-TPA, Py-TPADBO and Py-TPAMO dopants achieved maximum EQE values of 20.7%, 18.1% and 23.7%, respectively. Besides, Py-TPAMO-based devices realized a slow efficiency roll-off due to the fact that the fast RISC process reduced the triplet excited state concentration, further inhibiting the triplet–triplet annihilation process. Actually, only Py-TPAMO not only exhibits red-shifted emission spectra but also realizes higher device efficiency.

In summary, based on the introduction of electron-rich groups 1,4-benzodioxane and anisole into the prototypical TPA fragment, the donors TPADBO and TPAMO with strong electron-donating ability have been designed and synthesized. Accordingly, a series of TADF emitters Py-TPA, Py-TPADBO, and Py-TPAMO were tuned to obtain yellow, orange-red, and red emissions, respectively. Both theoretical calculations and experimental results clearly show that the HOMO energy levels of Py-TPADBO (−5.02 eV) and Py-TPAMO (−5.00 eV) are significantly increased by 0.3 eV compared to Py-TPA (−5.33 eV). As expected, the photophysical results show that the absorption and emission bands of Py-TPADBO and Py-TPAMO are slightly red-shifted due to the enhanced CT transition. Moreover, Py-TPAMO exhibits obvious advantages, *i.e.*, a small singlet-triplet energy gap and a small degree of excited-state deformation similar to that of the prototypical molecule Py-TPA, suggesting that TPAMO not only realizes the enhancement of the electron-donating ability but also does not bring negative effects. As a result, Py-TPAMO exhibits the best k_{nr}^S and k_{RISC} (2.21×10^6 s^{-1} and 1.33×10^5 s^{-1}, respectively). Surprisingly, the Py-TPAMO-based OLEDs achieve an increase in efficiency despite the red-shifted emission, with the maximum CE, PE and EQE of 47.7 cd/A, 40.4 lm/W and 25.5%, respectively. Overall, an efficient long-wavelength material requires stronger CT transition between donor and acceptor as well as slower severe non-radiative decay processes. We reported that the strong donor fragments can facilitate the further development of NIR-TADF emitters, in particular, the TPAMO fragments can provide strong electron-donating capability without inducing side effects. It is promised to be used in the construction of the long-wavelength emission and has achieved satisfactory performance. This work broadens the energy level range of donor fragments further providing diverse options for designing efficient long-wavelength TADF emitters.

Declaration of competing interest

The authors declare that they have no known competing financial interests or personal relationships that could have appeared to influence the work reported in this paper.

CRediT authorship contribution statement

Hao Zhuo: Writing – original draft, Investigation, Formal analysis, Data curation. **Ming Zhang:** Formal analysis, Data curation. **Hengyuan Zhang:** Investigation, Formal analysis. **Hui Lin:** Formal analysis. **Gang Yang:** Formal analysis. **Silu Tao:** Writing – review & editing, Formal analysis. **Caijun Zheng:** Writing – review & editing, Supervision, Project administration, Funding acquisition. **Xiaohong Zhang:** Writing – review & editing, Funding acquisition.

Acknowledgments

This work was supported by the National Natural Science Foundation of China (Nos. 62222503, 52073040 and 52130304), the Sichuan Science and Technology Program (Nos. 2024NSFSC0012, 2023NSFSC1973 and 2024NSFSC1446), the China Postdoctoral Science Foundation (Nos. 2023M740504 and GZC20230380), the Sichuan Provincial Human Resources and Social Security Department Program and the Collaborative Innovation Center of Suzhou Nano Science & Technology.

Supplementary materials

Supplementary material associated with this article can be found, in the online version, at doi:10.1016/j.cclet.2024.110760.

References

[1] G. Qian, Z.Y. Wang, Chem. Asian J. 5 (2010) 1006–1029.
[2] A. Zampetti, A. Minotto, F. Cacialli, Adv. Funct. Mater. 29 (2019) 1807623.
[3] M. Xu, X. Li, S. Liu, L. Zhang, W. Xie, Mater. Chem. Front. 7 (2023) 4744–4767.
[4] M.P. Zhuo, X.D. Wang, L.S. Liao, Small Sci. 2 (2022) 2200029.
[5] Y. Li, J.Y. Liu, Y.D. Zhao, Y.C. Cao, Mater. Today 20 (2017) 258–266.
[6] H. Xiang, J. Cheng, X. Ma, X. Zhou, J.J. Chruma, Chem. Soc. Rev. 42 (2013) 6128–6185.
[7] A. Minotto, I. Bulut, A.G. Rapidis, et al., Light: Sci. Appl. 10 (2021) 18.
[8] C. Wu, Y. Zhang, J. Miao, et al., Chin. Chem. Lett. 34 (2023) 107445.
[9] M. Zhang, C.J. Zheng, K. Wang, et al., Adv. Funct. Mater. 31 (2021) 2010100.
[10] Y. Zhang, D. Zhang, T. Huang, et al., Angew. Chem. Int. Ed. 60 (2021) 20498–20503.
[11] H. Uoyama, K. Goushi, K. Shizu, H. Nomura, C. Adachi, Nature 492 (2012) 234–238.
[12] H. Kaji, H. Suzuki, T. Fukushima, et al., Nat. Commun. 6 (2015) 8476.
[13] H.Y. Yang, H.Y. Zhang, M. Zhang, et al., Chem. Eng. J. 448 (2022) 137717.
[14] M. Zhang, W. Liu, C.J. Zheng, et al., Adv. Sci. 6 (2019) 1801938.
[15] M. Zhang, G. Dai, C. Zheng, et al., Chin. Chem. Lett. 33 (2022) 1110–1115.
[16] M. Zhang, C.J. Zheng, H. Lin, S.L. Tao, Mater. Horiz. 8 (2021) 401–425.
[17] Z.Q. Wang, W. Liu, C. Xu, et al., Opt. Mater. 58 (2016) 260–267.
[18] Z.Q. Wang, C.L. Liu, C.J. Zheng, et al., Org. Electron. 23 (2015) 179–185.
[19] H.Y. Yang, H.Y. Zhang, M. Zhang, et al., Chem. Eng. J. 468 (2023) 143721.
[20] Y. Xiao, H. Wang, Z. Xie, et al., Chem. Sci. 13 (2022) 8906–8923.
[21] J.V. Caspar, E.M. Kober, B.P. Sullivan, T.J. Meyer, J. Am. Chem. Soc. 104 (1982) 630–632.
[22] H.C. Li, X. Tang, S.Y. Yang, et al., Chin. Chem. Lett. 32 (2021) 1245–1248.
[23] J.H. Kim, J.H. Yun, J.Y. Lee, Adv. Opt. Mater. 6 (2018) 1800255.
[24] J.L. He, F.C. Kong, B. Sun, et al., Chem. Eng. J. 424 (2021) 130470.
[25] Y. Shen, X. Tang, Y. Xu, et al., Chin. Chem. Lett. 30 (2019) 1947–1950.
[26] X. Hu, Y. Qin, Z. Li, et al., Chin. Chem. Lett. 33 (2022) 4645–4648.
[27] X. Cao, D. Zhang, S. Zhang, Y. Tao, W. Huang, J. Mater. Chem. C 5 (2017) 7699–7714.
[28] W. Yang, W. Ning, H. Jungchi, et al., Chem. Eng. J. 438 (2022) 135571.
[29] J. Xue, Q. Liang, R. Wang, et al., Adv. Mater. 31 (2019) 1808242.
[30] J.X. Chen, H. Wang, Y.F. Xiao, et al., Small 18 (2022) 2201548.
[31] Z. Cai, X. Wu, H. Liu, et al., Angew. Chem. Int. Ed. 60 (2021) 23635–23640.
[32] S. Wang, Z. Cheng, X. Song, et al., ACS Appl. Mater. Interfaces 9 (2017) 9892–9901.
[33] S.H. Kim, J. Choi, C. Sakong, et al., Dyes Pigm. 113 (2015) 390–401.
[34] J. Xue, J. Xu, J. Ren, et al., Sci. China Chem. 64 (2021) 1786–1795.
[35] H. Wang, K. Wang, J.X. Chen, et al., Adv. Funct. Mater. 33 (2023) 2304398.
[36] J. Xue, J. Xu, Q. Liang, et al., Adv. Funct. Mater. 33 (2023) 2301312.
[37] Y.J. Yu, Y. Hu, S.Y. Yang, et al., Angew. Chem. Int. Ed. 59 (2020) 21578–21584.
[38] D.G. Congrave, B.H. Drummond, Q. Gu, et al., J. Mater. Chem. C 10 (2022) 4831–4836.
[39] H. Wang, J.X. Chen, L. Zhou, et al., Mater. Horiz. 10 (2023) 2997–3004.
[40] J. Fan, Y. Xu, N. Li, et al., J. Mater. Chem. C 10 (2022) 17059–17065.
[41] K. Sun, D. Liu, W. Tian, et al., J. Mater. Chem. C 8 (2020) 11850–11859.
[42] W. Yuan, D. Hu, M. Zhu, et al., Dyes Pigm. 191 (2021) 109395.
[43] R. Lin, J. Liu, W. Xu, et al., Adv. Mater. 35 (2023) 2303212.
[44] H.Y. Zhang, H.Y. Yang, M. Zhang, et al., Mater. Horiz. 9 (2022) 2425–2432.
[45] R. Ishimatsu, S. Matsunami, K. Shizu, et al., J. Mater. Chem. A 117 (2013) 5607–5612.
[46] W.C. Chen, B. Huang, S.F. Ni, et al., Adv. Funct. Mater. 29 (2019) 1903112.
[47] Y. Zhang, H.S. Pang, X.J. He, et al., J. Phys. Chem. C 124 (2020) 2782–2790.